LANGMUIR

pubs.acs.org/Langmuir Article

Operando X-ray Absorption Spectroscopy (XAS) Observation of Photoinduced Oxidation in FeNi (Oxy)hydroxide Overlayers on Hematite (α-Fe_2O_3) Photoanodes for Solar Water Splitting

Anton Tsyganok, Paolo Ghigna, Alessandro Minguzzi, Alberto Naldoni, Vadim Murzin, Wolfgang Caliebe, Avner Rothschild, and David S. Ellis*

Cite This: *Langmuir* 2020, 36, 11564–11572

Read Online

ACCESS | Metrics & More | Article Recommendations | Supporting Information

ABSTRACT: An FeNi (oxy)hydroxide cocatalyst overlayer was photoelectrochemically deposited on a thin-film hematite (α-Fe_2O_3) photoanode, leading to a cathodic shift of ~100 mV in the photocurrent onset potential. Operando X-ray absorption spectroscopy (XAS) at the Fe and Ni K-edges was used to study the changes in the overlayer with potential in the dark and under illumination conditions. Potential or illumination only had a minor effect on the Fe oxidation state, suggesting that Fe atoms do not accumulate significant amount of charge over the whole potential range. In contrast, the Ni K-edge spectra showed pronounced dependence on potential in the dark and under illumination. The effect of illumination is to shift the onset for the Ni oxidation because of the generated photovoltage and suggests that holes that are photogenerated in hematite are transferred mainly to the Ni atoms in the overlayer. The increase in the oxidation state of Ni proceeds at potentials corresponding to the redox wave of Ni, which occurs immediately prior to the onset of the oxygen evolution reaction (OER). Linear combination fitting analysis of the obtained spectra suggests that the overlayer does not have to be fully oxidized to promote oxygen evolution. Cathodic discharge measurements show that the photogenerated charge is stored almost exclusively in the Ni atoms within the volume of the overlayer.

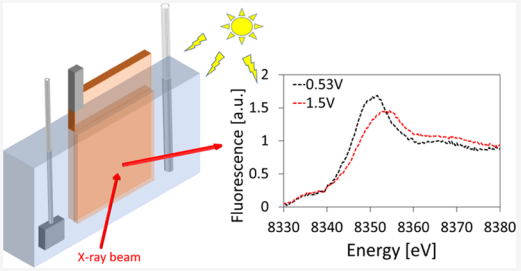

INTRODUCTION

Since the pioneering work of Fujishima and Honda in the early 1970s,[1] photoelectrochemical (PEC) water splitting has been actively investigated for its potential to provide an elegant path for the direct conversion of intermittent solar power into storable hydrogen fuel.[2] A notable candidate for a photoanode material that drives water photo-oxidation in PEC cells for solar water splitting is hematite (α-Fe_2O_3), being one of the few materials to meet the key criteria of stability, abundance, low cost, and a band gap suitable for effective sunlight absorption.[3] However, it also comes with some serious drawbacks: low mobility of charge carriers, low lifetime of photogenerated charge carriers due to bulk recombination, surface recombination at the photoanode/electrolyte interface, and high external voltage for solar-driven water splitting.[4−6] To address the last two issues, a widely exploited route to improve performance is to deposit various overlayers, which significantly reduce both surface recombination and the overpotential needed for water photo-oxidation.[7−9] NiFe (oxy)-hydroxide-based electrocatalysts are considered as favorable materials because of their inexpensive cost (abundant elements), high catalytic activity for the oxygen evolution reaction (OER),[10] and stability under water-oxidation reaction conditions in an alkaline solution.[11] There have been many studies of NiFe (oxy)hydroxide operating as a cocatalyst overlayer on top of a photoanode.[12−15] The resultant improvement in performance has been attributed to a variety of proposed mechanisms, including Fermi-level unpinning,[9] improved surface catalysis,[16] passivation of surface defects,[4] formation of a p−n junction,[17] or storage of excess holes to prevent surface recombination.[18] As was shown in previous studies,[18−20] the composition and fabrication method of the sample can have a profound effect on the role of the overlayer. Light-modulated impedance spectroscopy on Sn-doped hematite revealed that the addition of a NiFe (oxy)hydroxide overlayer caused a decrease of surface recombination as compared to the bare hematite sample, which improved sharply with potential in the vicinity of the photocurrent onset.[19] By measuring the electronic properties of a NiFe (oxy)hydroxide overlayer on hematite in situ, using a second working electrode, Qiu et al.[21] observed a dramatic rise in the electrical conductivity of the overlayer, spanning the Ni redox peak in the current−voltage curve, which immediately preceded the photocurrent onset. This, together with further

Received: July 14, 2020
Revised: September 8, 2020
Published: September 9, 2020

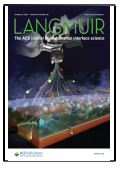

https://dx.doi.org/10.1021/acs.langmuir.0c02065
Langmuir 2020, 36, 11564−11572

in situ probing of the overlayer, led to the understanding that the overlayer is active for charge transfer from the hematite to the OER, only after it has been transformed into its oxidized and conductive state.

To further clarify the processes in the overlayer spectroscopically, herein we present a spectroelectrochemical study of the roles of Ni and Fe sites under operative conditions of PEC water splitting using X-ray absorption spectroscopy (XAS), an element-specific probe of the local structure, and oxidation state of atoms. Operando XAS, which can directly monitor changes in the oxidation state of catalytic sites in response to applied potential and/or illumination, has indeed been proven to be a powerful method for investigating charge-transfer processes in electrochemical and photoelectrochemical systems.[22,23] Braun et al., in their pioneering operando oxygen K-edge XAS study of a bare hematite photoanode under applied potential and illumination, interpreted pre-edge features as two types of holes at the hematite/electrolyte interface, which reached maximum population in the vicinity of the photocurrent onset.[24,25] A number of measurements were done on the metal absorption edge of overlayers deposited on photoabsorbers.[26−29] Minguzzi et al. performed an operando XAS study on an IrO_x overlayer deposited on top of a hematite photoanode, at the Ir K-edge, which showed clear oxidation of the Ir sites in response to illumination.[26] Li et al. used high-energy-resolution fluorescence detection XAS to study ultra-thin (1−3 nm) overlayers of IrO_x on top of a Si photoanode.[29] The authors observed a near-linear increase of the Ir oxidation state prior to the current onset, followed by saturation or even decrease a few hundreds of meV above the onset potential. Interestingly, these trends were completely identical for anodes that operate under light and dark conditions, aside from being shifted according to the respective onset potentials. This suggests that, for the hematite photoanode and NiFe (oxy)hydroxide overlayer system in the present study, previous operando XAS studies of NiFe (oxy)hydroxide catalysts, even without photoexcitation, could offer pertinent insights. Such (nonphoto) studies include recent papers by Friebel et al.,[30] Wang et al.,[31] and Drevon et al.,[32] and others.[33−35] Similar to the IrO_x overlayer studies,[26,29] the oxidation state of Ni was found to increase prior to the onset of the OER, and saturate a few hundreds of meV after the onset.[30−32] The Fe K-edge spectra, on the other hand, showed considerably less pronounced changes of oxidation state, although they were correlated with changes in Ni K-edge. By extracting bond lengths from extended X-ray fine structure (EXAFS) measurements, Friebel et al. found that Fe is not interstitial between NiO_2 sheets, but rather substitutes into Ni sites in NiO_6 octahedra at a low Fe content and additionally forms a separate γ-FeOOH phase at higher Fe content, and that the structure transforms from α-$Ni(OH)_2$ at low potential to γ-NiOOH upon oxygen evolution.[30] Recent work by Morikawa et al. on β-FeOOH nanorods modified with $Ni(OH)_2$ has suggested that β-NiOOH is the active phase under OER conditions.[36] While there have been no definite conclusions or consensus as to the precise roles of Fe and Ni in enhancing water-oxidation activity, which can also depend on the Fe/Ni ratio of the layer,[20] a decrease in the activation energy for OER at Fe sites as a result of shortening of the Fe−O bond length in NiFe (oxy)hydroxide was proposed as a possible mechanism. In this work, we measure a hematite photoanode with an FeNi (oxy)hydroxide overlayer (with ∼87 cat % Fe), with operando XAS at the Ni and Fe K-edges, controlling both potential and dark/light conditions, and discuss the results in the context of water photo-oxidation processes in PEC water splitting. We show the relation between the XAS results and photo-electrochemical measurements including current−voltage, and found a linear correspondence between the determined Ni oxidation state and cathodic discharge measurements.

EXPERIMENTAL SECTION

Our primary sample consisted of a heteroepitaxial Sn-doped (1 cat %) hematite layer, deposited by pulsed layer deposition on a Nb-doped SnO_2-coated (0001) sapphire substrate. The deposition conditions, layer structure, and microstructures of similar samples are reported elsewhere.[37] An FeNi (oxy)hydroxide cocatalyst overlayer with an Fe/Ni ratio of ∼7:1, to be consistent with our previous work,[19,38] was deposited photoelectrochemically on the hematite layer (note that the Fe−Ni order has been reversed to reflect a majority of Fe). Transmission electron microscopy (TEM) suggested the formation of two phases in the overlayer: an amorphous and a crystalline phase. The compositions of those phases cannot be resolved, but based on a previous report,[30] we speculate that one phase might be Ni(Fe)OOH, where some of the Ni sites are substituted by Fe, and the other phase is mostly a Ni-free FeOOH phase. Full characterization, including scanning electron microscopy (SEM), TEM, X-ray photoelectron spectroscopy (XPS), and atomic force microscopy (AFM) of similar samples, is reported in ref 19. A study of the effect of other Fe/Ni compositions on hematite could be a subject of future work. The thicknesses of the hematite layer and FeNi (oxy)hydroxide overlayer were estimated to be 10 and 30 nm, respectively. A bare hematite photoanode was prepared as a reference sample, under identical conditions, but without an overlayer. Linear sweep voltammetry (LSV) for both photoanodes, measured in the dark and under white-light illumination with an intensity of ∼100 mW/cm^2 at the sample position, is presented in Figure S1. The dark current was nearly zero over the entire potential range examined. Consistent with previous reports,[9,18,39] deposition of the FeNi (oxy)hydroxide cocatalyst overlayer led to a cathodic shift of ∼100 mV in the photocurrent onset potential, whereas the photocurrent plateau remained nearly the same as that for the bare hematite sample. However, unlike our previous study,[19] a small redox peak of Ni(II)/Ni(III) appeared at 1.05 V_{RHE} under illumination conditions, just before the onset potential for OER. The reason for the appearance of this peak is the relatively large thickness (∼30 nm) of the FeNi (oxy)hydroxide overlayer, designed to enhance its XAS signal, which was considerably thicker than that in the previous study (∼2 nm).

Figure 1 illustrates the configuration of the operando XAS measurements, which were performed at the P64 beamline of PETRA III synchrotron (DESY, Hamburg, Germany).[40] The sample was placed in a special electrochemical cell (see the SI for details),[27] such that a thin (∼200 to 300 μm) layer of 1 M NaOH aqueous electrolyte covered the sample surface. Potential was applied to the photoanode and the current was measured using an Ivium potentiostat in three-electrode mode, with a Hg/HgO/1 M NaOH reference electrode and a Pt counter electrode placed in the electrolyte. The sample was photoexcited with a high-power white light-emitting diode (LED) that provided an intensity of ∼100 mW/cm^2 at the sample position. For brevity, we denote this state of illumination as the "light" condition and absence of this as "dark". Fe and Ni K-edge absorption spectra were measured in fluorescence detection mode with a 100-pixel Ge-detector (Canberra). Further details including photographs of the cell and the measurement setup are provided in the SI (Figures S2 and S3). As a preliminary check for possible beam damage to the sample and to ensure stability of the PEC system, successive measurements of the XAS spectrum of the bare hematite sample near the Fe K-edge were carried out in dark, light, and back to dark conditions, at a constant potential of 1.5 V_{RHE}, where there is photocurrent. Figure S4 shows that the white line (WL) intensity decreased under light conditions, which is likely associated with partial oxidation of surface Fe sites[31,32] that proceeds under oxygen evolution conditions.[41,42] Upon removing the

https://dx.doi.org/10.1021/acs.langmuir.0c02065
Langmuir 2020, 36, 11564−11572

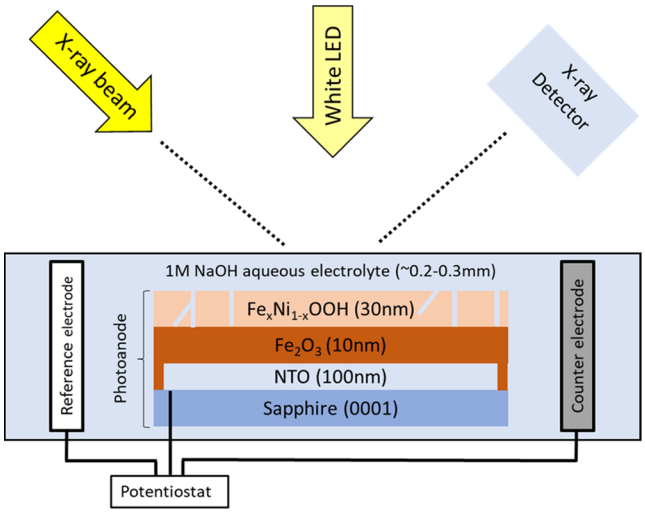

Figure 1. Schematic top-view illustration of the operando photoelectrochemical XAS measurement setup.

illumination and returning to dark conditions, the spectrum was restored to its initial dark state, demonstrating the stability of the system.

The procedure to monitor the evolution of oxidation states of Fe and Ni in the photoanode was as follows: the potential was set to values tracing the photocurrent pre-onset (points A, B) and post-onset (points C, D, E) regions of the LSV curve (under illumination) shown in Figure 2. A zoom-in of the dark current, presented in the

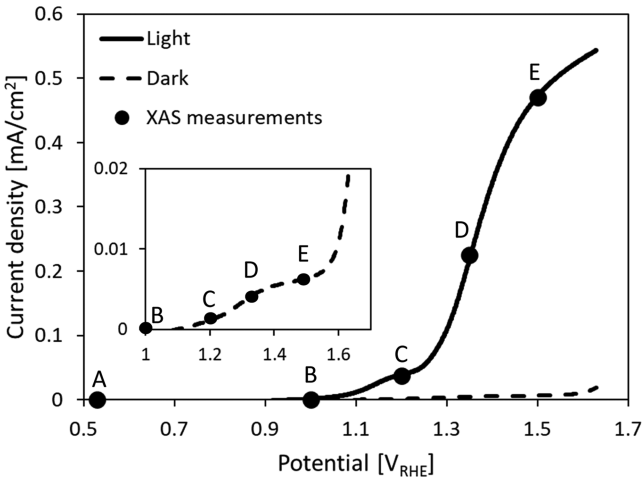

Figure 2. LSV voltammograms measured under dark (dashed line) and light (solid line) conditions within the beamline before the XAS measurements for hematite/FeNi (oxy)hydroxide. Points A–E represent XAS measurement points taken under the light condition. XAS measurements were carried out also in the dark at the same potential values. Note that we use the same labels for the corresponding potentials under dark conditions. Inset: Zoom-in of the dark current LSV.

inset of Figure 2, reveals a feature related to Ni redox activity,[43,44] prior to the onset of oxygen evolution. For each potential, and for both dark and light conditions, XAS spectra were measured at both the Fe and Ni K-edges, before proceeding to the next potential. The near-edge spectra for the Fe K-edge are shown in Figure 3a,b for dark and light conditions, respectively. Note that all of the spectra presented here were normalized by the standard procedure using Athena software,[45] according to the jump at the absorption edge, defined by the difference between the extrapolated lines fitted to the

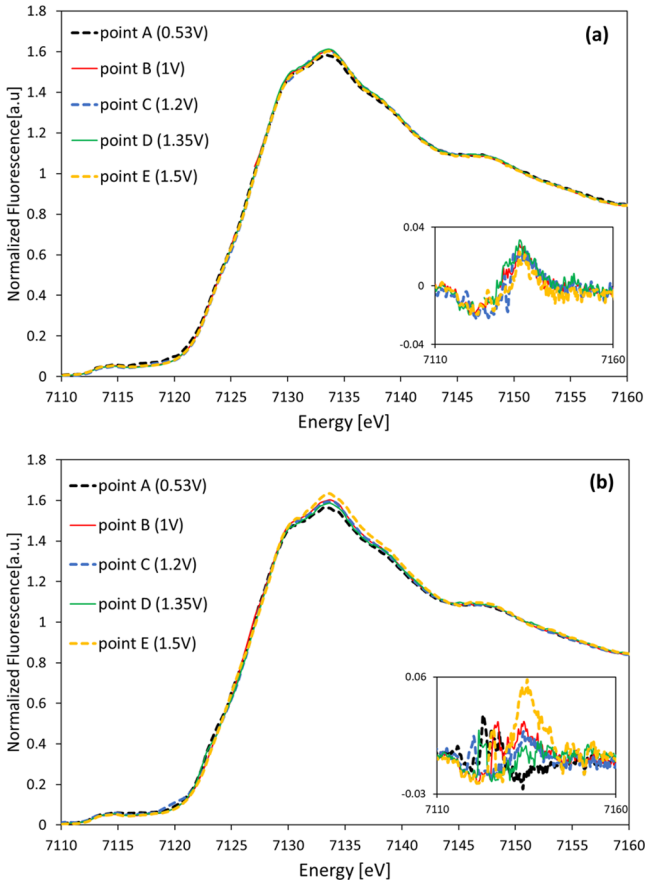

Figure 3. Normalized Fe K-edge XANES spectra of hematite/FeNi (oxy)hydroxide under (a) dark and (b) light conditions. The measurement point, at different potentials (see Figure 2), is indicated in the legend. All of the potentials are versus RHE. All of the spectra are normalized by the standard method based on the extrapolated jump at the absorption edge. The insets show the measured spectra subtracted by the spectrum measured in point A (0.53 V_{RHE}) in the dark.

low-energy (pre-edge) and high-energy (post-edge) parts of the spectra. As is common practice, the WL intensity is described relative to this jump.

RESULTS

We focus on the near-edge (XANES) region since most of the clear changes were observed there. Full spectra are presented in Figure S5. From Figure 3a, the XAS spectra measured in the dark, with the exception of point A (at 0.53 V_{RHE}), were affected very little by the applied potential in the range applied. To highlight any differences between the spectra, the insets in Figure 3 show them subtracted by the spectrum measured at point A (0.53 V_{RHE}) in the dark. All of the spectra are characterized by a shift in spectral weight to higher energies (manifested by a negative valley, followed by a positive peak), as compared to the spectrum measured at point A (0.53 V_{RHE}), but were otherwise independent of potential. We suggest that the spectral weight shift common to points B–E is related to the expected depletion of electrons from the surface at anodic bias.[42] Under illumination (Figure 3b), the general trend is similar to that of the dark case, except for a notable increase in the intensity of the WL peak for point E (1.5 V_{RHE}). The spiky features observed in the insets of Figure 3 originate from the tails of the Bragg peaks that were not completely removed

https://dx.doi.org/10.1021/acs.langmuir.0c02065
Langmuir 2020, 36, 11564–11572

from the data (see the SI for more details). No other significant potential dependences in the XANES or EXAFS region (shown in Figure S5) of the spectra were detected. This result of very little (if any) oxidation of Fe atoms is generally consistent with previous reports of relatively small oxidation of Fe in FeNi (oxy)hydroxide electrocatalysts.[30−32,46] Furthermore, the contribution from the underlying hematite layer would diminish observed changes in the Fe-edge spectra originating from the overlayer. It is peculiar that the WL of the Fe K-edge under illumination slightly increases with potential, rather than decreases as might have been expected from electrocatalyst studies.[30−32] In fact, it is difficult to distinguish Fe contributions coming from the FeNi (oxy)hydroxide overlayer or the hematite layer. However, we note that the trend is opposite to that observed for bare hematite in Figure S4. We speculate that the origin of this effect might be a change in the geometry, or a small change in the time-averaged Fe oxidation state, of the Fe sites in the overlayer as a result of a change in the oxidation state of neighboring Ni sites,[30,35] or some additional effect of illumination on the overlayer that EXAFS analysis could possibly clarify, but will be investigated elsewhere. Whatever the case, the relatively small changes indicate that most of the Fe sites of the overlayer do not accumulate charge before and during OER.

The XAS spectra at the Ni K-edge, under dark and light conditions, are presented in Figure 4, displaying markedly more pronounced changes than those observed for the Fe K-edge spectra in Figure 3. Increase of the Ni oxidation state with increased potentials is evident from the shifts in the WL for both dark and light conditions. Notably, the oxidation state of Ni also increases in the dark (Figure 4a), just below the OER onset potential, at potentials encompassing the broad peak at ∼1.35 V (Figure 2, inset). This is not surprising, since the standard potential of the Ni(II)/Ni(III) ($Ni(OH)_2$/NiOOH) redox reaction is 1.348 V.[47] It is also consistent with the study of Drevon et al., who reported an edge shift prior to the OER onset in NiFe (oxy)hydroxide electrocatalysts,[32] as well as Li et al. for Si photoabsorbers with Ir overlayers.[29] Most of the change in the WL region occurs between the spectra recorded at points C (1.2 V_{RHE}, blue curve) and D (1.35 V_{RHE}, green curve), while the spectrum recorded at point E (1.5 V_{RHE}, orange curve) nearly overlaps with that recorded at point D. This indicates that the Ni oxidation begins to saturate just after the onset of OER current (Figure 2, inset), consistent with previous reports on NiFe (oxy)hydroxide electrocatalysts.[30,32] Fitting of the spectra, shown below, can clarify the oxidation state trends.

Under illumination conditions (Figure 4b), the WL shift is even more pronounced. The most noticeable change in the XANES region is observed between the spectra recorded at points B (1 V_{RHE}, red solid curve) and C (1.2 V_{RHE}, blue curve), near the onset potentials of Ni photo-oxidation and prior to water photo-oxidation (at ∼1.2 V_{RHE}) observed in the LSV curve measured under illumination. The spectral shift begins to stabilize around point D (1.35 V_{RHE}). Comparison of the light and dark spectra at each potential (Figure S5) clearly shows that starting at point C (1.2 V_{RHE}), illumination shifts the WL position to higher energies. This is likely a result of photogenerated holes injected from the hematite layer into the FeNi (oxy)hydroxide overlayer. Indeed, most of the photogenerated holes produced in the photoanode originate in the hematite layer, made evident from the greater optical absorption in the hematite layer.[16,19,48] In contrast to the

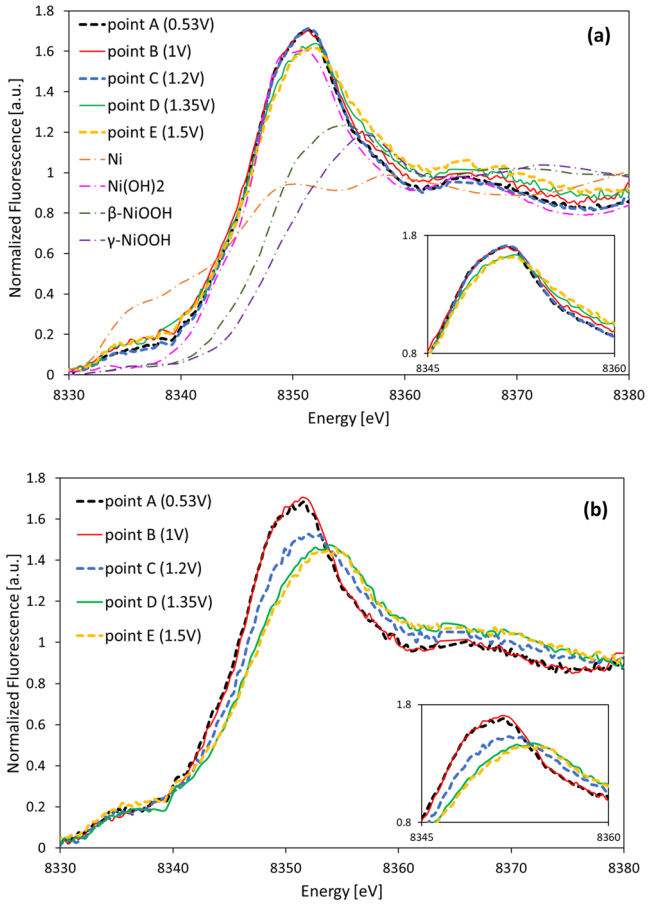

Figure 4. Normalized Ni K-edge XANES spectra for hematite/FeNi (oxy)hydroxide under (a) dark and (b) light conditions. The measurement point, at different potentials (see Figure 2), is indicated in the legend. All of the potentials are versus RHE. All of the spectra are normalized by the standard method based on the extrapolated jump at the absorption edge. Normalized Ni K-edge XANES spectra for NiO, β-NiOOH, and Ni standards used for the fitting are also presented in panel (a). Inset: Zoom-in of the WL region.

hole injection under illumination, conduction band electrons are responsible for charge transfer in the dark, in the case of n-type Sn-doped hematite photoanodes.[49] Combining the results obtained in dark and light conditions, it follows that both electrons and holes can be transferred between the hematite layer and the FeNi (oxy)hydroxide overlayer. The transfer of the photogenerated holes to the overlayer also suppresses surface recombination,[4,18] as was also suggested by intensity-modulated photocurrent spectroscopy (IMPS) measurements for similar samples.[19]

To clarify the trend of the average Ni oxidation state as a function of applied potential under dark and light conditions, we fit each of the measured spectra to a sum of XAS spectra of Ni, $Ni(OH)_2$, β-NiOOH, and γ-NiOOH, as standards for the Ni(O), Ni(II), Ni(III), and higher (>Ni(III)) oxidation states, respectively. These standards were selected based on the most stable phases in the Pourbaix diagram of Ni under the measurement conditions (not considering the presence of Fe).[50] γ-NiOOH is known to have a mixed Ni(III)/Ni(IV) oxidation state[51] and therefore can be used as a standard for higher oxidation states. The relative weights of the components were obtained by a least-squares fitting routine using the Levenberg−Marquardt method. The fitting method and

https://dx.doi.org/10.1021/acs.langmuir.0c02065
Langmuir 2020, 36, 11564−11572

results, and choice of standards, are described in more detail in the SI. The normalized XAS spectra of these standards are plotted in Figure 4a. A Ni standard was used for the fitting process because a pre-edge feature was observed in all of the spectra at ∼8335 eV, which is a typical signature of metallic nickel (Ni(0)).[52] Subsequent to the XAS measurements, SEM−energy-dispersive spectrometry (EDS) analysis showed the presence of metallic Ni on the electrical contact clips to the sample (Figure S6 in SI), which may have contributed to the observed spectra. It was also determined from fitting that the metallic Ni contribution of the spectra was largely independent of potential or light (24 ± 1%). Therefore, assuming a constant contribution from the connectors, all of the spectra were fitted simultaneously while keeping the metallic Ni fraction as a shared parameter among all of the spectra. The resultant fit curves are shown in Figure S7.

According to the fits, most of the Ni oxidized to a phase resembling β-NiOOH, but for the highest two potentials under illumination (points D and E), an ∼15% spectral content of γ-NiOOH was observed. This latter observation is in line with previous studies of NiFe (oxy)hydroxides that reported the formation of γ-NiOOH under overcharging conditions.[53−56] The average oxidation state of Ni in the sample was calculated according to the obtained fractions of the Ni phases (+2 for NiO, +3 for β-NiOOH, and +3.6 for γ-NiOOH), excluding metallic Ni contribution. Plotted in Figure 5, the average

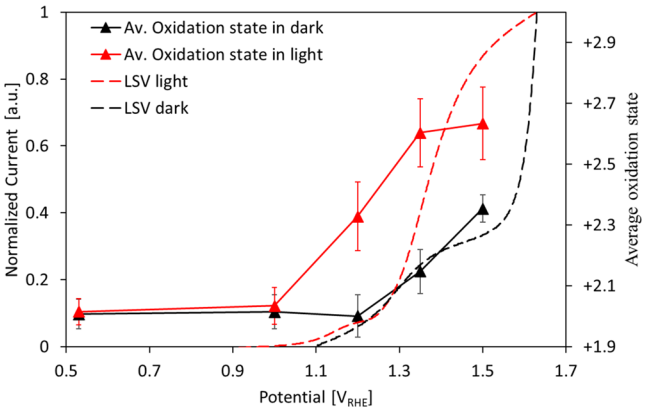

Figure 5. Average oxidation state of Ni under dark (solid line with black triangles) and light (solid line with red triangles) conditions for hematite/FeNi (oxy)hydroxide, overlaid on the LSV voltammograms recorded during the XAS measurement under the same conditions (black and dashed lines are for dark and light conditions, respectively). Dark and light currents were normalized by dividing by their respective currents at 1.63 V_{RHE}.

oxidation state is overlaid on normalized LSV curves in the dark and light. In the dark condition, the oxidation state of Ni is +2 up to ∼1.2 V_{RHE}, above which it gradually increases to an average oxidation state of +2.35 at a potential of 1.53 V_{RHE}, corresponding to a state of charge (SOC) of 35% in the transition from Ni(II) to Ni(III). For measurements under illumination, the onset of Ni (photo)-oxidation shifts to a lower potential than that in the dark, with the oxidation state increasing rapidly above ∼1 V_{RHE}, corresponding to the onset of the Ni redox wave in the LSV curve, and below the onset of the OER. We note that for both light and dark conditions, the linear region of Ni oxidation increase occurs at the potentials spanning the Ni redox wave in the respective LSV curves. The Ni oxidation curves in the light and dark seem similar but shifted according to the respective shift of the LSV curves, considered to be the photovoltage generated in the photoanode.[57] A similar photovoltage-related shift was observed by Li et al.[29] At the highest applied potential in light (1.5 V_{RHE}), the average oxidation state reaches a value of +2.6, where it begins to saturate. These observations are in line with previous reports that partial oxidation and transition from the hydroxide to the oxyhydroxide phase precedes the OER and then saturates prior to the plateau region in the water photo-oxidation current.[29,30,35]

The effect of a similar overlayer was previously studied by our group by means of IMPS, and it was found that the main effect was to reduce the surface recombination at potentials above the photocurrent onset potential.[19] Other studies have attributed the reduction in surface recombination to passivation of the surface recombination centers,[4] catalyzing the OER,[20,41] or charge separation.[18] The correlation between the onset of the photocurrent and nickel photo-oxidation in Figure 5 suggests that the FeNi (oxy)hydroxide overlayer functions as a charge storage layer that separates the holes stored in the overlayer from the electrons in the hematite layer, thereby reducing the surface recombination that delays the photocurrent onset in bare hematite.[19] The mechanism of catalyzing OER or the surface passivation can proceed in parallel with the charge separation and cannot be ruled out based on the obtained data. Figure 5 shows that the overlayer does not need to be fully oxidized to reduce the recombination, consistent with the electrochemical measurements reported by Qiu et al.[21] However, we cannot rule out the possibility that the foremost surface atoms may be fully oxidized, since the X-ray fluorescence includes contributions from many atomic layers. The observed saturation of the oxidation state not far above the onset for OER could be owing to competition for holes between Ni and water-oxidation reactions. When the overlayer is charged to its active state, a portion of the holes begin to be injected into the electrolyte, while the remainder continue to cause oxidation of the overlayer. This would create negative feedback, since if oxidized Ni enhances the OER, this increased OER will draw more holes away from further increasing its oxidation state, therefore stabilizing (saturating) it at some potential.

As a complementary investigation of how the overlayer transforms during the OER, cathodic discharge measurements were carried out for the samples with and without the FeNi (oxy)hydroxide overlayer. These measurements determine "stable charge", which does not get discharged upon removing light, but only by ramping down potential. The measurement procedure, as first proposed to monitor the surface state in TiO_2 photoanodes for water photo-oxidation,[58] was also previously applied to study hematite photoanodes.[37,59,60] The sample is first held in the electrolyte (1 M NaOH) under a constant potential (called the charging potential) and illumination, to facilitate filling of hematite surface states and charge the FeNi (oxy)hydroxide overlayer. In the next step, the light is turned off, and the current drops. After the current has stabilized, the potential is swept cathodically to discharge the surface states and the FeNi (oxy)hydroxide overlayer. The resulting cathodic current upon discharge is integrated over time to calculate the "stable" charge that remained after the light was turned off. A representative cathodic discharge measurement plot is shown in Figure S10. The resultant stable charge as a function of the applied charging potential for bare hematite photoanode and hematite photoanode with the FeNi

https://dx.doi.org/10.1021/acs.langmuir.0c02065
Langmuir 2020, 36, 11564−11572

(oxy)hydroxide overlayer is plotted in Figure 6a. The amount of stored charge in the sample with the FeNi (oxy)hydroxide

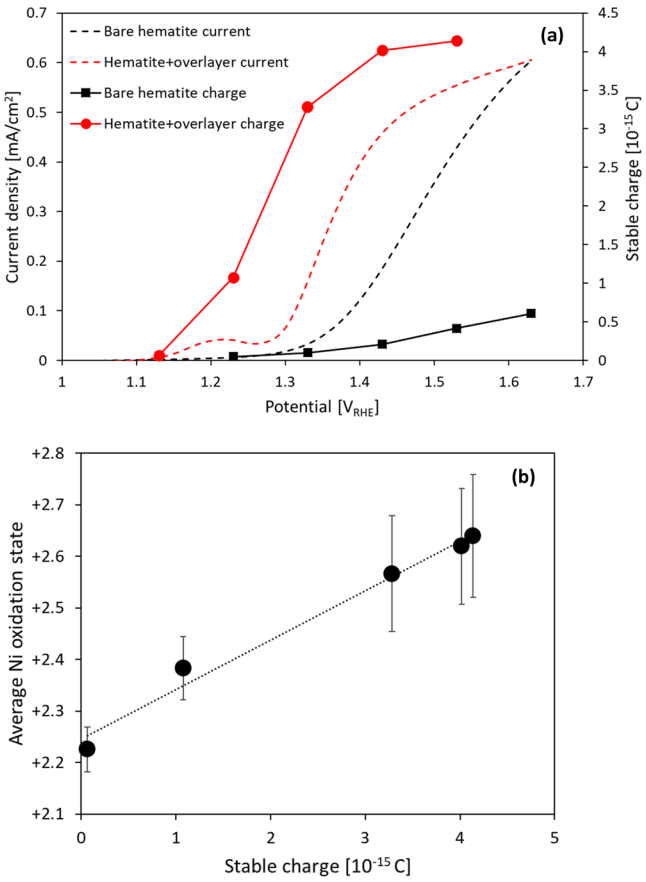

Figure 6. (a) Stable charge for bare hematite (black squares) and hematite/FeNi (oxy)hydroxide photoanodes (red circles), as a function of charging potential, overlaid on LSV measurement under matching conditions for bare hematite (black dashed line) and hematite with an overlayer (red dashed line). (b) Average Ni oxidation state under illumination (obtained from XAS fitting) as a function of the stable charge for the hematite photoanode with the overlayer, interpolated from Figure 5 and (a).

overlayer is an order of magnitude higher than that for the bare hematite. This is because the charge is stored only on the surface in the case of the bare hematite photoanode, while in the case of an ion-permeable redox-active layer such as the FeNi (oxy)hydroxide overlayer, the charge is stored in the whole layer. A similar observation was made for a "nonstable charge" measurement of the transient currents in response to light on/off at a potential fixed to the OER onset,[39] which is also related to stable charge.[61] For bare hematite, a strong correlation between the photocurrent and stable surface charge curves is observed, consistent with a previous study,[61] suggesting a direct correlation between the two processes. However, a distinctly different trend is observed for the sample with the FeNi (oxy)hydroxide overlayer. Major accumulation of charge instead coincides with the onset potential of Ni photo-oxidation that occurs *prior* to the onset of OER. Moreover, the stable charge curve is similar to the oxidation state curve (Figure 5). Figure 6b shows the interpolated average oxidation state as a function of the stored stable charge. The plot suggests linear dependence between the two parameters, supporting accumulation of the stable charge by oxidation of the Ni atoms. We note that the Ni oxidation state for zero stable charge is higher than +2. The reason is that most of the charge accumulated at low potentials is in the form of "unstable" charge, which is removed upon switching off the light during stable charge measurements.[39,61] The obtained data shows that Ni sites are oxidized by the photogenerated holes, even before the onset of water photo-oxidation. The stable charge seems to stabilize at the highest potential applied (1.5 V_{RHE}), in line with the stabilization of the Ni oxidation state obtained from the XAS measurements.

CONCLUSIONS

To summarize, we have studied the effect of illumination and potential on the oxidation of the transition metal sites (Fe, Ni) in the hematite photoanode with an FeNi (oxy)hydroxide overlayer. The observed change with potential for the Fe K-edge was rather small; however, it was more pronounced for light than for dark conditions. This small change of the average could signify a temporary increase in the Fe oxidation state. It would be of great interest for future studies to track the evolution of possible oxidation states with time, which could be connected to multiple-site reactions (in this case, Ni and Fe) as recently suggested in the literature.[62−64] The Ni sites were more strongly affected by both potential and illumination, consistent with previous spectroelectrochemical operando XAS studies, including those done without photoexcitation.[29−32] For both dark and light conditions, we found that partial oxidation of Ni in the overlayer proceeded at potentials corresponding to the redox wave of Ni ($Ni(OH)_2/NiOOH$), which occurs immediately prior to the onset of the OER. This is consistent with the picture of Qiu et al;[21] the Ni sites need to be oxidized for effective OER activity. The reduction of the recombination current, observed using IMPS,[19] coincides with the oxidation of the Ni in the overlayer. These observations further suggest that the main effect of light absorption is to shift the Ni oxidation to lower potentials by the photovoltage generated in the photoanode. The maximal oxidation state of Ni started to saturate and reached a value of +2.6 ± 0.1 under illumination, and a negative feedback mechanism limiting the oxidation state was suggested. In addition, considering the dependence of the Ni K-edge on potential in the dark and light, we conclude that both electrons and holes can be transferred between the hematite and FeNi (oxy)hydroxide layers. Intriguingly, the cathodic discharge measurements shared very similar characteristics to the Ni oxidation state curve (from XAS measurements), rather than the photocurrent curve as for bare hematite, showing a linear relation to phase transformations in the overlayer. We observed a greater than 10-fold increase of stable charge measured for the sample with the FeNi (oxy)hydroxide overlayer, as compared to the bare hematite sample, indicating that the whole overlayer stores the charge in the Ni atoms, consistent with the XAS results. While the iron atoms did not appear to be charged on average, it does not rule out the possibility that their oxidation state could change in some temporal window in the transient response to illumination. Future advances in instrumentation could enable such dynamical measurements to be resolved in the temporal and/or spatial domains.

ASSOCIATED CONTENT

Supporting Information

The Supporting Information is available free of charge at https://pubs.acs.org/doi/10.1021/acs.langmuir.0c02065.

https://dx.doi.org/10.1021/acs.langmuir.0c02065
Langmuir 2020, 36, 11564−11572

Sample preparation and characterization; measurement setup details; details of the XAS measurement setup and cell; XAS stability test of the bare hematite sample; full XAS data; XAS fitting procedure and error analysis details; and cathodic discharge measurement description (PDF)

AUTHOR INFORMATION

Corresponding Author

David S. Ellis − *Department of Materials Science and Engineering, Technion—-Israel Institute of Technology, Haifa 3200003, Israel;* orcid.org/0000-0002-7639-3264; Email: ellis@technion.ac.il

Authors

Anton Tsyganok − *Department of Materials Science and Engineering, Technion—-Israel Institute of Technology, Haifa 3200003, Israel*

Paolo Ghigna − *Dipartimento di Chimica, Università di Pavia, and Unità INSTM di Pavia, I2700 Pavia, Italy;* orcid.org/0000-0002-8680-7272

Alessandro Minguzzi − *Regional Centre of Advanced Technologies and Materials, Faculty of Science, Palacký University Olomouc, 771 46 Olomouc, Czech Republic;* orcid.org/0000-0002-8130-4465

Alberto Naldoni − *Dipartimento di Chimica, Università degli Studi di Milano, 20133 Milano, Italy;* orcid.org/0000-0001-5932-2125

Vadim Murzin − *Deutsches Elektonen-Synchrotron DESY, 22603 Hamburg, Germany; Bergische Universität Wuppertal, 42119 Wuppertal, Germany;* orcid.org/0000-0003-2743-8398

Wolfgang Caliebe − *Deutsches Elektonen-Synchrotron DESY, 22603 Hamburg, Germany*

Avner Rothschild − *Department of Materials Science and Engineering, Technion—-Israel Institute of Technology, Haifa 3200003, Israel;* orcid.org/0000-0002-2512-0370

Complete contact information is available at: https://pubs.acs.org/10.1021/acs.langmuir.0c02065

Notes

The authors declare no competing financial interest.

ACKNOWLEDGMENTS

This research was carried out at the P64 Advanced EXAFS beamline at DESY, a member of the Helmholtz Association (HGF). We would like to thank Tayal Akhil for assistance during the experiment. A.T. would like to thank Dr. Alex Mehlmann for his expert help in advance preparation prior to the beamtime measurements. The beamtime measurements were supported by the project CALIPSOplus under the Grant Agreement 730872 from the EU Framework Programme for Research and Innovation HORIZON 2020. The research leading to these results has received funding from the European Research Council under the European Union's Seventh Framework programme (FP/2007−2013)/ERC (grant agreement no. 617516) and from the PAT Center of Research Excellence supported by the Israel Science Foundation (grant no. 1867/17). A.T. acknowledges the generous financial support from the Israel Ministry of Energy as a part of the scholarship program in the field of energy (219-01-044). A.N. gratefully acknowledges the support of the Operational Programme Research, Development, and Education−European Regional Development Fund, project no. CZ.02.1.01/0.0/0.0/15_003/0000416, of the Ministry of Education, Youth and Sports of the Czech Republic. V.M. acknowledges the generous financial support from the BMBF project 05K19PXA.

REFERENCES

(1) Fujishima, A.; Honda, K. Electrochemical Photolysis of Water at a Semiconductor Electrode. *Nature* **1972**, *238*, 37−38.

(2) Walter, M. G.; Warren, E. L.; McKone, J. R.; Boettcher, S. W.; Mi, Q.; Santori, E. A.; Lewis, N. S. Solar Water Splitting Cells. *Chem. Rev.* **2010**, *110*, 6446−6473.

(3) Sivula, K.; Le Formal, F.; Grätzel, M. Solar Water Splitting: Progress Using Hematite (α-Fe(2) O(3)) Photoelectrodes. *ChemSusChem* **2011**, *4*, 432−449.

(4) Thorne, J. E.; Jang, J.-W.; Liu, E. Y.; Wang, D. Understanding the Origin of Photoelectrode Performance Enhancement by Probing Surface Kinetics. *Chem. Sci.* **2016**, *7*, 3347−3354.

(5) Cowan, A. J.; Barnett, C. J.; Pendlebury, S. R.; Barroso, M.; Sivula, K.; Grätzel, M.; Durrant, J. R.; Klug, D. R. Activation Energies for the Rate-Limiting Step in Water Photooxidation by Nanostructured α-Fe2O3 Nd TiO2. *J. Am. Chem. Soc.* **2011**, *133*, 10134−10140.

(6) Dare-Edwards, M. P.; Goodenough, J. B.; Hamnett, A.; Trevellick, P. R. Electrochemistry and Photoelectrochemistry of Iron(III) Oxide. *J. Chem. Soc., Faraday Trans. 1* **1983**, *79*, No. 2027.

(7) Tilley, S. D.; Cornuz, M.; Sivula, K.; Grätzel, M. Light-Induced Water Splitting with Hematite: Improved Nanostructure and Iridium Oxide Catalysis. *Angew. Chem.* **2010**, *122*, 6549−6552.

(8) Carroll, G. M.; Gamelin, D. R. Kinetic Analysis of Photoelectrochemical Water Oxidation by Mesostructured Co-Pi/α-Fe2O3 Photoanodes. *J. Mater. Chem. A* **2016**, *4*, 2986−2994.

(9) Du, C.; Yang, X.; Mayer, M. T.; Hoyt, H.; Xie, J.; McMahon, G.; Bischoping, G.; Wang, D. Hematite-Based Water Splitting with Low Turn-On Voltages. *Angew. Chem., Int. Ed.* **2013**, *52*, 12692−12695.

(10) Fidelsky, V.; Toroker, M. C. The Secret behind the Success of Doping Nickel Oxyhydroxide with Iron. *Phys. Chem. Chem. Phys.* **2017**, *19*, 7491−7497.

(11) Roger, I.; Shipman, M. A.; Symes, M. D. Earth-Abundant Catalysts for Electrochemical and Photoelectrochemical Water Splitting. *Nat. Rev. Chem.* **2017**, No. 0003.

(12) Lin, F.; Boettcher, S. W. Adaptive Semiconductor/Electrocatalyst Junctions in Water-Splitting Photoanodes. *Nat. Mater.* **2014**, *13*, 81−86.

(13) Malara, F.; Fabbri, F.; Marelli, M.; Naldoni, A. Controlling the Surface Energetics and Kinetics of Hematite Photoanodes Through Few Atomic Layers of NiO $_x$. *ACS Catal.* **2016**, *6*, 3619−3628.

(14) Stevens, M. B.; Trang, C. D. M.; Enman, L. J.; Deng, J.; Boettcher, S. W. Reactive Fe-Sites in Ni/Fe (Oxy)Hydroxide Are Responsible for Exceptional Oxygen Electrocatalysis Activity. *J. Am. Chem. Soc.* **2017**, *139*, 11361−11364.

(15) Riha, S. C.; Klahr, B. M.; Tyo, E. C.; Seifert, S.; Vajda, S.; Pellin, M. J.; Hamann, T. W.; Martinson, A. B. F. Atomic Layer Deposition of a Submonolayer Catalyst for the Enhanced Photoelectrochemical Performance of Water Oxidation with Hematite. *ACS Nano* **2013**, *7*, 2396−2405.

(16) Morales-Guio, C. G.; Mayer, M. T.; Yella, A.; Tilley, S. D.; Grätzel, M.; Hu, X. An Optically Transparent Iron Nickel Oxide Catalyst for Solar Water Splitting. *J. Am. Chem. Soc.* **2015**, *137*, 9927−9936.

(17) Zandi, O.; Hamann, T. W. The Potential versus Current State of Water Splitting with Hematite. *Phys. Chem. Chem. Phys.* **2015**, *17*, 22485−22503.

(18) Hajibabaei, H.; Schon, A. R.; Hamann, T. W. Interface Control of Photoelectrochemical Water Oxidation Performance with Ni 1−x Fe x O y Modified Hematite Photoanodes. *Chem. Mater.* **2017**, *29*, 6674−6683.

(19) Tsyganok, A.; Klotz, D.; Malviya, K. D.; Rothschild, A.; Grave, D. A. Different Roles of Fe 1− x Ni x OOH Cocatalyst on Hematite (α-Fe 2 O 3) Photoanodes with Different Dopants. *ACS Catal.* **2018**, *8*, 2754−2759.
(20) Francàs, L.; Corby, S.; Selim, S.; Lee, D.; Mesa, C. A.; Godin, R.; Pastor, E.; Stephens, I. E. L.; Choi, K. S.; Durrant, J. R. Spectroelectrochemical Study of Water Oxidation on Nickel and Iron Oxyhydroxide Electrocatalysts. *Nat. Commun.* **2019**, *10*, No. 5208.
(21) Qiu, J.; Hajibabaei, H.; Nellist, M. R.; Laskowski, F. A. L.; Hamann, T. W.; Boettcher, S. W. Direct in Situ Measurement of Charge Transfer Processes during Photoelectrochemical Water Oxidation on Catalyzed Hematite. *ACS Cent. Sci.* **2017**, *3*, 1015−1025.
(22) Fabbri, E.; Abbott, D. F.; Nachtegaal, M.; Schmidt, T. J. Operando X-Ray Absorption Spectroscopy: A Powerful Tool toward Water Splitting Catalyst Development. In *Current Opinion in Electrochemistry*; Elsevier B.V, 2017; pp 20−26.
(23) Deng, J.; Zhang, Q.; Lv, X.; Zhang, D.; Xu, H.; Ma, D.; Zhong, J. Understanding Photoelectrochemical Water Oxidation with X-Ray Absorption Spectroscopy. *ACS Energy Lett.* **2020**, *5*, 975−993.
(24) Braun, A.; Sivula, K.; Bora, D. K.; Zhu, J.; Zhang, L.; Grätzel, M.; Guo, J.; Constable, E. C. Direct Observation of Two Electron Holes in a Hematite Photoanode during Photoelectrochemical Water Splitting. *J. Phys. Chem. C* **2012**, *116*, 16870−16875.
(25) Braun, A.; Hu, Y.; Boudoire, F.; Bora, D. K.; Sarma, D. D. D.; Grätzel, M.; Eggleston, C. M. The Electronic, Chemical and Electrocatalytic Processes and Intermediates on Iron Oxide Surfaces during Photoelectrochemical Water Splitting. *Catal. Today* **2016**, *260*, 72−81.
(26) Minguzzi, A.; Naldoni, A.; Lugaresi, O.; Achilli, E.; D'Acapito, F.; Malara, F.; Locatelli, C.; Vertova, A.; Rondinini, S.; Ghigna, P. Observation of Charge Transfer Cascades in α-Fe_2O_3/IrO_x Photoanodes by Operando X-Ray Absorption Spectroscopy. *Phys. Chem. Chem. Phys.* **2017**, *19*, 5715−5720.
(27) Fracchia, M.; Cristino, V.; Vertova, A.; Rondinini, S.; Caramori, S.; Ghigna, P.; Minguzzi, A. Operando X-Ray Absorption Spectroscopy of WO3 Photoanodes. *Electrochim. Acta* **2019**, *320*, No. 134561.
(28) Xi, L.; Schwanke, C.; Zhou, D.; Drevon, D.; Van De Krol, R.; Lange, K. M. In Situ XAS Study of CoBi Modified Hematite Photoanodes. *Dalton Trans.* **2017**, *46*, 15719−15726.
(29) Li, L.; Yang, J.; Ali-Löytty, H.; Weng, T. C.; Toma, F. M.; Sokaras, D.; Sharp, I. D.; Nilsson, A. Operando Observation of Chemical Transformations of Iridium Oxide during Photoelectrochemical Water Oxidation. *ACS Appl. Energy Mater.* **2019**, *2*, 1371−1379.
(30) Friebel, D.; Louie, M. W.; Bajdich, M.; Sanwald, K. E.; Cai, Y.; Wise, A. M.; Cheng, M. J.; Sokaras, D.; Weng, T. C.; Alonso-Mori, R.; et al. Identification of Highly Active Fe Sites in (Ni,Fe)OOH for Electrocatalytic Water Splitting. *J. Am. Chem. Soc.* **2015**, *137*, 1305−1313.
(31) Wang, D.; Zhou, J.; Hu, Y.; Yang, J.; Han, N.; Li, Y.; Sham, T. K. In Situ X-Ray Absorption Near-Edge Structure Study of Advanced NiFe(OH)x Electrocatalyst on Carbon Paper for Water Oxidation. *J. Phys. Chem. C* **2015**, *119*, 19573−19583.
(32) Drevon, D.; Görlin, M.; Chernev, P.; Xi, L.; Dau, H.; Lange, K. M. Uncovering The Role of Oxygen in Ni-Fe(OxHy) Electrocatalysts Using In Situ Soft X-Ray Absorption Spectroscopy during the Oxygen Evolution Reaction. *Sci. Rep.* **2019**, *9*, No. 1532.
(33) Bediako, D. K.; Lassalle-Kaiser, B.; Surendranath, Y.; Yano, J.; Yachandra, V. K.; Nocera, D. G. Structure-Activity Correlations in a Nickel-Borate Oxygen Evolution Catalyst. *J. Am. Chem. Soc.* **2012**, *134*, 6801−6809.
(34) Yoshida, M.; Mitsutomi, Y.; Mineo, T.; Nagasaka, M.; Yuzawa, H.; Kosugi, N.; Kondoh, H. Direct Observation of Active Nickel Oxide Cluster in Nickel-Borate Electrocatalyst for Water Oxidation by in Situ O K-Edge X-Ray Absorption Spectroscopy. *J. Phys. Chem. C* **2015**, *119*, 19279−19286.
(35) González-Flores, D.; Klingan, K.; Chernev, P.; Loos, S.; Mohammadi, M. R.; Pasquini, C.; Kubella, P.; Zaharieva, I.; Smith, R. D. L.; Dau, H. Nickel-Iron Catalysts for Electrochemical Water Oxidation-Redox Synergism Investigated by: In Situ X-Ray Spectroscopy with Millisecond Time Resolution. *Sustainable Energy Fuels* **2018**, *2*, 1986−1994.
(36) Morikawa, T.; Gul, S.; Nishimura, Y. F.; Suzuki, T. M.; Yano, J. Operando X-Ray Absorption Spectroscopy of Hyperfine β-FeOOH Nanorods Modified with Amorphous Ni(OH)2 under Electrocatalytic Water Oxidation Conditions. *Chem. Commun.* **2020**, *56*, 5158−5161.
(37) Grave, D. A.; Klotz, D.; Kay, A.; Dotan, H.; Gupta, B.; Visoly-Fisher, I.; Rothschild, A. Effect of Orientation on Bulk and Surface Properties of Sn-Doped Hematite (α-Fe $_2$ O $_3$) Heteroepitaxial Thin Film Photoanodes. *J. Phys. Chem. C* **2016**, *120*, 28961−28970.
(38) Tsyganok, A. Effect of Fe(1-x)Ni(x)OOH Overlayer on Photo-Electrochemical Performance of Hematie (Alpha-Fe2O3) Photoandes. M.Sc. Thesis, Technion, 2018.
(39) Young, K. M. H.; Hamann, T. W. Enhanced Photocatalytic Water Oxidation Efficiency with Ni(OH) 2 Catalysts Deposited on α-Fe 2 O 3 via ALD. *Chem. Commun.* **2014**, *50*, 8727−8730.
(40) Caliebe, W. A.; Murzin, V.; Kalinko, A.; Görlitz, M. In *High-Flux XAFS-Beamline P64 at PETRA III*, AIP Conference Proceedings; American Institute of Physics Inc., 2019; Vol. 2054, 060031.
(41) Le Formal, F.; Pastor, E.; Tilley, S. D.; Mesa, C. A.; Pendlebury, S. R.; Grätzel, M.; Durrant, J. R. Rate Law Analysis of Water Oxidation on a Hematite Surface. *J. Am. Chem. Soc.* **2015**, *137*, 6629−6637.
(42) Zandi, O.; Hamann, T. W. Determination of Photoelectrochemical Water Oxidation Intermediates on Haematite Electrode Surfaces Using Operando Infrared Spectroscopy. *Nat. Chem.* **2016**, *8*, 778−783.
(43) Smith, R. D. L.; Berlinguette, C. P. Accounting for the Dynamic Oxidative Behavior of Nickel Anodes. *J. Am. Chem. Soc.* **2016**, *138*, 1561−1567.
(44) Smith, R. D. L. L.; Prévot, M. S.; Fagan, R. D.; Zhang, Z.; Sedach, P. A.; Siu, M. K. J.; Trudel, S.; Berlinguette, C. P. Photochemical Route for Accessing Amorphous Metal Oxide Materials for Water Oxidation Catalysis. *Science* **2013**, *340*, 60−63.
(45) Ravel, B.; Newville, M. ATHENA, ARTEMIS, HEPHAESTUS: Data Analysis for X-Ray Absorption Spectroscopy Using IFEFFI. *J. Synchrotron Radiat.* **2005**, *12*, 537−541.
(46) Görlin, M.; Chernev, P.; De Araújo, J. F.; Reier, T.; Dresp, S.; Paul, B.; Krähnert, R.; Dau, H.; Strasser, P. Oxygen Evolution Reaction Dynamics, Faradaic Charge Efficiency, and the Active Metal Redox States of Ni-Fe Oxide Water Splitting Electrocatalysts. *J. Am. Chem. Soc.* **2016**, *138*, 5603−5614.
(47) Bratsch, S. G. Standard Electrode Potentials and Temperature Coefficients in Water at 298.15 K. *J. Phys. Chem. Ref. Data* **1989**, *18*, 1−21.
(48) Piekner, Y.; Dotan, H.; Tsyganok, A.; Malviya, K. D.; Grave, D. A.; Kfir, O.; Rothschild, A. Implementing Strong Interference in Ultrathin Film Top Absorbers for Tandem Solar Cells. *ACS Photonics* **2018**, *5*, 5068−5078.
(49) Kay, A.; Grave, D. A.; Ellis, D. S.; Dotan, H.; Rothschild, A. Heterogeneous Doping to Improve the Performance of Thin-Film Hematite Photoanodes for Solar Water Splitting. *ACS Energy Lett.* **2016**, *1*, 827−833.
(50) Beverskog, B.; Puigdomenech, I. Revised Pourbaix Diagrams for Nickel at 25−300 °C. *Corros. Sci.* **1997**, *39*, 969−980.
(51) Van der Ven, A.; Morgan, D.; Meng, Y. S.; Ceder, G. Phase Stability of Nickel Hydroxides and Oxyhydroxides. *J. Electrochem. Soc.* **2006**, *153*, A210.
(52) Marco, J. F.; Gancedo, J. R.; Gracia, M.; Gautier, J. L.; Ríos, E.; Berry, F. J. Characterization of the Nickel Cobaltite, NiCo2O4, Prepared by Several Methods: An XRD, XANES, EXAFS, and XPS Study. *J. Solid State Chem.* **2000**, *153*, 74−81.
(53) Bode, H.; Dehmelt, K.; Witte, J. Zur Kenntnis Der Nickelhydroxidelektrode-I. Über Das Nickel (II)-Hydroxidhydrat. *Electrochim. Acta* **1966**, *11*, 1079−1087.
(54) Klaus, S.; Cai, Y.; Louie, M. W.; Trotochaud, L.; Bell, A. T. Effects of Fe Electrolyte Impurities on Ni(OH)2/NiOOH Structure

and Oxygen Evolution Activity. *J. Phys. Chem. C* **2015**, *119*, 7243−7254.
(55) Lyons, M. E. G.; Brandon, M. P. *The Oxygen Evolution Reaction on Passive Oxide Covered Transition Metal Electrodes in Aqueous Alkaline Solution*. Part 1-Nickel; Electrochemical Science Group, 2008; Vol. 3.
(56) Oshchepkov, A. G.; Braesch, G.; Bonnefont, A.; Savinova, E. R.; Chatenet, M. Recent Advances in the Understanding of Ni-Based Catalysts for the Oxidation of Hydrogen-Containing Fuels in Alkaline Media. *ACS Catal.* **2020**, 7043−7068.
(57) Dotan, H.; Mathews, N.; Hisatomi, T.; Grätzel, M.; Rothschild, A. On the Solar to Hydrogen Conversion Efficiency of Photoelectrodes for Water Splitting. *J. Phys. Chem. Lett.* **2014**, 3330−3334.
(58) Wilson, R. H. Observation and Analysis of Surface States on TiO[Sub 2] Electrodes in Aqueous Electrolytes. *J. Electrochem. Soc.* **1980**, *127*, 228.
(59) Klahr, B.; Gimenez, S.; Fabregat-Santiago, F.; Bisquert, J.; Hamann, T. W. Electrochemical and Photoelectrochemical Investigation of Water Oxidation with Hematite Electrodes. *Energy Environ. Sci.* **2012**, *5*, 7626.
(60) Klahr, B.; Hamann, T. Water Oxidation on Hematite Photoelectrodes: Insight into the Nature of Surface States through in Situ Spectroelectrochemistry. *J. Phys. Chem. C* **2014**, *118*, 10393−10399.
(61) Natav, Y.; Caspary-Toroker, M.; Rothschild, A. *A Combined Experimental and Theoretical Investigation Of Iron-Oxide Photoelectrodes for Water Splitting*; PhD Thesis, Technion, 2019.
(62) Avital, Y. Y.; Dotan, H.; Klotz, D.; Grave, D. A.; Tsyganok, A.; Gupta, B.; Kolusheva, S.; Visoly-Fisher, I.; Rothschild, A.; Yochelis, A. Two-Site H2O2 Photo-Oxidation on Haematite Photoanodes. *Nat. Commun.* **2018**, *9*, No. 4060.
(63) Vandichel, M.; Busch, M.; Laasonen, K. Oxygen Evolution on Metal-oxy-hydroxides: Beneficial Role of Mixing Fe, Co, Ni Explained via Bifunctional Edge/Acceptor Route. *ChemCatChem* **2020**, *12*, 1436−1442.
(64) Song, F.; Busch, M. M.; Lassalle-Kaiser, B.; Hsu, C. S.; Petkucheva, E.; Bensimon, M.; Chen, H. M.; Corminboeuf, C.; Hu, X. An Unconventional Iron Nickel Catalyst for the Oxygen Evolution Reaction. *ACS Cent. Sci.* **2019**, *5*, 558−568.

https://dx.doi.org/10.1021/acs.langmuir.0c02065
Langmuir 2020, 36, 11564−11572